All-Optical Switching and Router via the Direct Quantum Control of Coupling between Cavity Modes

Keyu Xia (夏可宇)* and Jason Twamley

ARC Centre for Engineered Quantum Systems, Department of Physics and Astronomy, Macquarie University, New South Wales 2109, Australia

(Received 26 November 2012; revised manuscript received 23 June 2013; published 5 September 2013)

In this work, we describe a scheme to execute all-optical control of the routing or switching of photonic information where, by optically controlling the internal quantum state of a individual scatterer coupled to two independent cavity modes, one can dynamically and rapidly modulate the intermode coupling. This allows all-optical modulation of intercavity couplings via ac Stark or shuffle (stimulated Raman adiabatic passage) control of the scatterer's internal states, and from this modulation, we show that we can perform all-optical switching and all-optical routing with near-unit switching contrast and with high bandwidth.

DOI: 10.1103/PhysRevX.3.031013 Subject Areas: Condensed Matter Physics, Photonics, Quantum Physics

I. INTRODUCTION

The dynamic control of the interaction between optical cavity modes is essential for the advanced functioning of photonic and quantum photonic devices such as optical delay based on the optical analog of electromagnetically induced transparency [1–3], all-optical switching [4], and all-optical routing [5,6]. Popular methods to control the couplings between cavity modes involve tuning the cavity resonance either by laser-assisted carrier-induced nonlinearities [1,7–9] or by thermal-optical effects [2]. By detuning two cavities out of resonance with each other, one can indirectly decouple two cavity modes that are arranged to strongly couple when on resonance. However, tuning methods that rely on media possessing a small nonlinear refractive index require intense optical control fields. An interaction between cavity modes can also be controlled slowly by moving a scatterer [10] or by tuning a spatial gap between the cavities [2,3]. All of the current methods to modulate the coupling between separate optical cavities suffer from various drawbacks; i.e., they are slow, may require nonlinear optical media, do not operate at the single-photon level, and require sophisticated physical setups, etc. In the following, we propose a new scheme, via controlling a three-level scatterer placed within or nearby a cavity, that allows rapid all-optical control of cavity couplings and permits the routing of optical signals (including single photons) between multiple cavities and via these cavities into many input-output waveguides with nearly perfect switching fidelity. Our proposal is essentially different from previous methods in that we are able to directly modulate the coherent intermode interaction strength.

*keyu.xia@mq.edu.au

Routing of photons plays a key role in optical communication networks and quantum information processing. One can demonstrate all-optical switching via the saturation of a single emitter in a cavity [11,12], but the contrast achieved is very low. The aforementioned method of tuning the resonance of a nonlinear optical cavity [7,9,13,14] or the evanescent coupling between waveguides [15] with an intense laser has been proposed for all-optical switching and routing, but these methods require high-pump-laser powers due to the very weak optical nonlinearity. By using a high-Q cavity or a high carrier-induced nonlinearity, one can decrease the intensity of the pump laser, but these methods also slow down the switching speed, as either the cavity exhibits a long ring-down time [14] or the carrier relaxation time becomes very long [1,9].

Cavity quantum electrodynamics (cQED) offers a powerful toolkit to control the transmission of light through a cavity or waveguide system where the cavity resonantly interacts with an emitter or scatterer [4–6,16]. A single scatterer strongly coupled to a one-dimensional waveguide can scatter a single photon in the waveguide into either the forward (transmission) or the backward (reflection) mode [17,18]. This discovery has been used to propose a single-photon transistor [19,20]. However, previous cQED schemes using on-resonance interaction with a single emitter and single-photon transistor only allow one to route a single photon into either the forward path or the backward path. To date, multiport all-optical routers formed from the composition of two-port routers [15] or optical switches [9] suffer from large insertion losses, in particular, when extended to provide multipath routing. Although the formalism of a Λ-type atomic scatterer interacting with a cavity mode has been widely studied [18,21–23], using this three-level system to dynamically modulate the coupling between cavities has never been addressed, to the best of our knowledge.

In this paper, we theoretically propose a method to control the coupling (or coherent scattering) between two optical cavity modes using a Λ-type three-level

system (scatterer) that dispersively interacts with both cavity modes simultaneously in the strong-coupling regime. This dispersive coupling induces a coherent interaction between the two cavity modes that depends on the common detuning and the quantum state of the scatterer. To modulate the strength of this intercavity coupling, we must thus develop ways to either control the size of the common detuning or directly change the internal quantum state of the scatterer. We show how both of these control routes are possible. We show that one can modulate the interaction strength by (i) tuning the detuning via an optical Stark shift or (ii) transferring [via stimulated Raman adiabatic passage (STIRAP) [24]] one internal ground state of the scatterer to another internal ground state, which does not interact with either cavity, to effectively turn off the intercavity coupling. We show that both methods can rapidly switch on or off the coupling between the two cavity modes with very high (near-unit) switching contrast. This control also allows for the dynamic cancellation of scattering in a toroidal cavity if the dynamic coupling is set to be the same number of the scattering but the opposite sign.

II. SETUP

Before discussing in detail the setup for optical switching and routing, we explain the basic idea behind our method. In summary, we show that when two optical modes with identical frequencies couple to the same transition in the Λ system, these two modes are indirectly coupled together.

Now, we go on to find an expression for the strength of this coupling and see that one can modulate this strength in two ways. As a potential photonic crystal realization, we refer to Fig. 1 and consider how one can create a tunable coherent coupling between two cavity modes using a Λ-type three-level system [e.g., a single nitrogen-vacancy (NV) center in a nanodiamond or a quantum dot] denoting the three level's internal energies and associated quantum eigenstates as ω_j and $|j\rangle$, $j \in \{1, 2, 3\}$. We arrange for two cavity modes $\hat{a}$ and $\hat{b}$ to simultaneously off-resonantly couple to the transition $|1\rangle \leftrightarrow |3\rangle$ with the coupling strengths $g_{a/b}$. We assume that these two modes have identical frequencies and thus suffer identical detunings, i.e., $\Delta_a = \Delta_b = \Delta$, and couple identically to the qubit, i.e., $g_a = g_b = g$. We observe that both quantum fields $\hat{a}$ and $\hat{b}$ induce Stark shifts on levels $|1\rangle$ and $|3\rangle$. The value of this shift $\Delta^{(13)}_{\text{Stark}}$ is given by $\Delta^{(13)}_{\text{Stark}} = |g|^2\langle(\hat{a}^\dagger + \hat{b}^\dagger)(\hat{a} + \hat{b})\rangle/\Delta$. In the situation of $|\Delta|^2 \gg |g|^2\langle\hat{a}^\dagger\hat{a}\rangle, |g|^2\langle\hat{b}^\dagger\hat{b}\rangle$, state $|3\rangle$ is negligibly populated, i.e., $\langle\sigma_{33}\rangle \sim 0$, where we set $\hat{\sigma}_{ij} = |i\rangle\langle j|$ with $i, j \in \{1, 2, 3\}$. This Stark shift effectively yields a coherent interaction $h(\hat{a}^\dagger\hat{b} + \hat{b}^\dagger\hat{a})$ between the two cavity modes with a strength

$$h = |g|^2\langle\hat{\sigma}_{11}\rangle/\Delta, \tag{1}$$

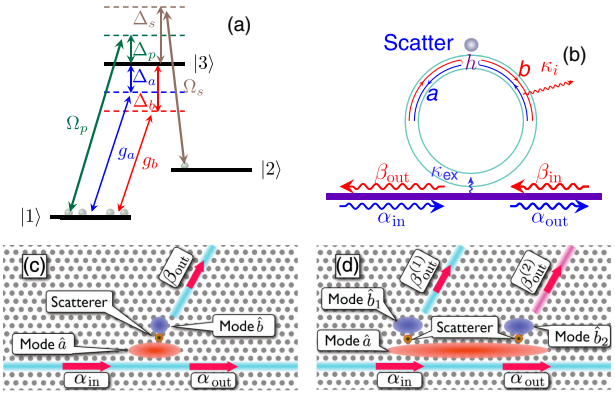

FIG. 1. Control of switching and routing via a Λ-type qubit interacting with a cavity. By controlling the three-level system, we can alter the transmission of the combined qubit-cavity system. (a) Energy level diagram of a Λ-type three-level scatterer. Two cavity modes $\hat{a}$ and $\hat{b}$ drive the same transition $|1\rangle \leftrightarrow |3\rangle$ with strength and detuning $\{g_a, \Delta_a\}$ and $\{g_b, \Delta_b\}$, respectively. The classical field $\Omega_p(\Omega_s)$ drives transition $|1\rangle \leftrightarrow |3\rangle$ ($|2\rangle \leftrightarrow |3\rangle$) with detuning $\Delta_p(\Delta_s)$. The field Ω_s shifts the energy of level $|3\rangle$ or in combination with Ω_p is used to swap quantum states between $|1\rangle$ and $|2\rangle$. (b) Optical switching via the control of the transmission. The waveguide overcouples to the cavity. Via tuning the coherent coupling h created by the scatterer (the Λ-type qubit), both forward and backward transmissions T_a and T_b can be switched on or off. (c) Optical router to control the output path. The photonic crystal cavity $\hat{a}$ couples to a one-dimensional waveguide. The coupling between two photonic crystal cavities a and b is controlled by a scatterer such as a NV center or a quantum dot. (d) The setup for an all-optical router. The cavity $\hat{a}$ can individually couple to each cavity $\hat{b}_l$ mediated by the individual scatterers. The field stored in cavity $\hat{b}_l$ couples out to the lth waveguide β_l.

and it is this expression that is at the crux of our scheme. From Eq. (1), we see that to tune the strength of this coupling, we can either (A) change Δ (via the Stark effect), which we denote as Stark control, or (B) change the value of $\langle\hat{\sigma}_{11}\rangle$ (via shuffling around the internal population of the Λ system), which we denote as shuffling control. To achieve (A), we must temporally change the detuning Δ, and this change of tuning can be achieved by using a strong classical optical field on the $|2\rangle \leftrightarrow |3\rangle$ to impose a large ac Stark shift on $|3\rangle$. To achieve (B), we propose using classical optical fields to shuffle the internal state $|1\rangle \leftrightarrow |2\rangle$, and when the entire internal population is in state $|2\rangle$, then $\langle\hat{\sigma}_{11}\rangle = 0$ and the cavity coupling is effectively switched completely off.

The two degenerate coupled-cavity modes could either be two counterpropagating modes of a ring resonator [see Fig. 1(b)] or two photonic crystal-cavity modes [see Fig. 1(c)]. In addition, tunable coupling enables photon routing. This capability to route can be seen in the following manner: Since we can control the interaction between two cavities, we can selectively transfer the field energy from one cavity to another and then feed it into the selected output waveguide. Using a waveguide to input or output

the field from the cavity, a realization of an all-optical router can be suggested, as shown in Fig. 1(d). We use tilted oriented waveguides to optimally output fields from the cavities $\hat{b}$ [25].

III. MODEL

Now, we discuss in some detail the general setup shown in Fig. 1(d), where we choose the router output among the ports $\alpha_{\rm out}$ and $\beta^{(l)}_{\rm out}$. After going to the frame defined by the unitary transformation $\hat{U}=\exp\{-i\omega_{\rm in}t\hat{a}^\dagger\hat{a}-i\sum_l[\omega_{\rm in}\hat{b}^\dagger_l\hat{b}_l+\in_3\hat{\sigma}^{(l)}_{33}+(\in_3-\omega_{\rm in})\hat{\sigma}^{(l)}_{11}+(\in_3-\omega_s)\hat{\sigma}^{(l)}_{22}]t\}$ and making the rotating-wave approximation, the dynamics for the system can be written in the form

$$\frac{\partial\langle\hat{Q}\rangle}{\partial t}=i\langle[\hat{H},\hat{Q}]\rangle+\hat{\mathcal{L}}\hat{Q}_q+\hat{\mathcal{L}}\hat{Q}_r, \tag{2}$$

with

$$\hat{H}=\hat{H}_{\rm in}+\hat{H}_0+\hat{H}_{\rm cc}+\hat{H}_{\rm sc}+\hat{H}_{\rm c}, \tag{3a}$$

$$\hat{H}_{\rm in}=i\sqrt{2\kappa_{\rm ex}}(\alpha_{\rm in}\hat{a}^\dagger-\alpha^*_{\rm in}\hat{a}), \tag{3b}$$

$$\hat{H}_0=-\sum_l[(\Delta^{(l)}_a+\Delta_{\rm in})\hat{\sigma}^{(l)}_{11}+\Delta^{(l)}_s\hat{\sigma}^{(l)}_{22}]+\Delta_{\rm in}\hat{a}^\dagger\hat{a}+\sum_l(\Delta_{\rm in}+\delta_l)\hat{b}^\dagger_l\hat{b}_l, \tag{3c}$$

$$\hat{H}_{\rm cc}=\sum_l h^{(l)}_0(\hat{a}^\dagger\hat{b}_l+\hat{b}^\dagger_l\hat{a}), \tag{3d}$$

$$\hat{H}_{\rm sc}=\sum_l\hat{\sigma}^{(l)}_{31}(g_a\hat{a}+g^{(l)}_b\hat{b}_l)+{\rm H.c.}, \tag{3e}$$

$$\hat{H}_{\rm c}=\sum_l[\Omega^{(l)}_p(t)e^{-i\tilde{\Delta}^{(l)}_p t}\hat{\sigma}^{(l)}_{13}+\Omega^{(l)}_s(t)\hat{\sigma}^{(l)}_{23}]+{\rm H.c.}, \tag{3f}$$

where $\hat{Q}$ denotes any operator within the enlarged system of scatterer and modes, and $\langle\cdot\rangle$ denotes the quantum average value of an operator. $\hat{\mathcal{L}}\hat{Q}_{q/r}$ describes the decoherence of the scatterer or cavities. For ease of reading, the various terms in Eq. (3) are described in detail in Table I.

We also model the decay of the scatterer and cavities via the Linblads in Eq. (4). We assume that the excited state $|3\rangle_l$ of the lth scatterer decays to the ground state $|j\rangle$ ($j\in\{1,2\}$) at the rate $\gamma^{(l)}_{3j}$, while we assume decay rates κ_A for cavity modes A ($A\in\{\hat{a},\hat{b}_l\}$) ($\hbar=1$):

$$\hat{\mathcal{L}}\hat{Q}_q=\frac{\gamma_{3j}}{2}\{2\langle\hat{\sigma}^{(l)}_{3j}\hat{Q}\hat{\sigma}^{(l)}_{j3}\rangle-\langle\hat{Q}\hat{\sigma}^{(l)}_{33}\rangle-\langle\hat{\sigma}^{(l)}_{33}\hat{Q}\rangle\}, \tag{4a}$$

$$\hat{\mathcal{L}}\hat{Q}_r=\frac{\kappa_A}{2}\{2\langle\hat{A}^\dagger\hat{Q}\hat{A}^\dagger\rangle-\langle\hat{Q}\hat{A}^\dagger\hat{A}\rangle-\langle\hat{A}^\dagger\hat{A}\,\hat{Q}\rangle\}. \tag{4b}$$

The decay rate κ_A of each cavity consists of two contributions, $\kappa_A=\kappa^{(a)}_i+\kappa_{\rm ex}$ for cavity a and $\kappa_A=\kappa^{(l)}_i+\kappa^{(l)}_{\rm ex}$ for b_l. $\kappa^{(a)}_i(\kappa^{(l)}_i)$ represents the intrinsic loss in cavity $a(b_l)$, while $\kappa^{(l)}_{\rm ex}$ describes loss due to the coupling of modes $a(b_l)$ to waveguides.

The overlap of the cavity evanescent fields with the waveguides leads to a coupling that is dependent on their gap, which is normally fixed. Only the cavity mode $\hat{a}$ couples to the input waveguide with strength $\kappa_{\rm ex}$. There is also bare cross-talk coupling between the cavities, i.e., in the absence of any scatterers. The $\hat{a}$ mode couples to the lth cavity $\hat{b}_l$ with strength $h^{(l)}_0$. Both of these strengths can be adjusted by engineering the spacing between the waveguides or cavities. However, for our scatterer-mediated modulation to be fast, we require that the bare intercavity cross-talk coupling is much smaller that the coupling by each cavity to the scatterer. To achieve small cross talk is obviously not easy, but we suggest a method to do this in the later section on implementation.

Our goal is to optically control the effective couplings $h_l=g_a g^*_{b_l}\langle\hat{\sigma}^{(l)}_{11}\rangle/\Delta^{(l)}_a$ via the application of classical coherent fields $\Omega^{(l)}_{p,s}$ that are selectively applied to implement one of the above-mentioned tuning methods: (A) Stark tuning is implemented by shifting the transition frequency of the lth scatterer or (B) Shuffle tuning is implemented by implementing STIRAP shuffling of the scatterer's internal population [24].

According to the input-output relation of an optical cavity [5,26–28], the output field operators for the $\hat{a}$ and $\hat{b}_l$ cavities are given in terms of the input and intracavity field operators as

$$\hat{a}_{\rm out}=-\hat{a}_{\rm in}+\sqrt{2\kappa_{\rm ex}}\hat{a}(t), \tag{5a}$$

$$\hat{b}^{(l)}_{\rm out}=-\hat{b}^{(l)}_{\rm in}+\sqrt{2\kappa^{(l)}_{\rm ex}}\hat{b}_l(t), \tag{5b}$$

where $[\hat{A}(t),\hat{A}^\dagger(t')]=\delta(t-t')$ with $\hat{A}=\{\hat{a}_{\text{in-out}},\hat{b}^{(l)}_{\text{in-out}}\}$, and $\kappa^{(l)}_{\rm ex}$ is an extrinsic contribution to the decay rate from cavity $\hat{b}_l$ due to coupling to the output $\beta^{(l)}_{\rm out}$. The coherent amplitudes of the input fields are given by $\langle\hat{a}_{\rm in}\rangle=\alpha_{\rm in}$ and $\langle\hat{b}^{(l)}_{\rm in}\rangle=0$. The transmission amplitudes are defined here as $t_a=\langle\hat{a}_{\rm out}\rangle/\alpha_{\rm in}$ and $t_l=\langle\hat{b}^{(l)}_{\rm out}\rangle/\alpha_{\rm in}$. Therefore, the corresponding transmission coefficients are $T_a(T_l)=|t_a|^2(|t_l|^2)$ for a coherent input $\alpha_{\rm in}$.

Both optical switching and routing rely on the realization of coupling between cavities $\hat{a}$ and $\hat{b}_l$. Compared with an optical router with multiple ports, it is much easier to realize an optical switch. For a switch, we have only one $\hat{b}$ mode and one scatterer. The setup is depicted either via Fig. 1(b) or Fig. 1(c). As a natural extension of optical switching, an all-optical router can be realized using the setup shown in Fig. 1(d), where many cavities $\hat{b}_l$ couple to the main cavity mode $\hat{a}$. The coupling strength h_l is individually modulated by the lth scatterer. Each cavity $\hat{b}_l$ couples out to a unique output waveguide that forms an output port $\beta^{(l)}_{\rm out}$. Thus, the input field $\alpha_{\rm in}$ can be routed into various output waveguides via the intermediate cavities $\hat{a}$ and $\hat{b}$.

For a transparent description of how one can engineer a coherent interaction between cavity modes $\hat{a}$ and $\hat{b}$, we first adiabatically eliminate the internal excited state $|3\rangle$ of the

TABLE I. Description of Hamiltonians.

Input	$\hat{H}_{\rm in}$	Represents the driving of the cavity mode $\hat{a}$ with resonant frequency ω_a via the input field $\alpha_{\rm in}$ of frequency $\omega_{\rm in}$ through the waveguide, where $\alpha_{\rm in}$ corresponds to the coherent amplitude of the input field and $\kappa_{\rm ex}$ describes the extrinsic loss due to coupling of the modes to the waveguides.
Self-energy	$\hat{H}_0$	Is the free Hamiltonian of the cavity mode $\hat{a}$ and output modes $\hat{b}_l$, where the latter modes have resonant frequencies $\omega_b^{(l)}$. Relative to the incoming drive, the $\hat{a}$ mode is detuned by $\Delta_{\rm in} = \omega_a - \omega_{\rm in}$ and the $b^{(l)}$ mode by $\Delta_{\rm in} + \delta_l$, with $\delta_l = \omega_b^{(l)} - \omega_a$. $\hat{H}_0$ also includes the free energy of the two ground states of all of the l scatterers with the detunings $\Delta_a^{(l)} = \in_3^{(l)} - \in_1^{(l)} - \omega_a$ and $\Delta_s^{(l)} = \in_3^{(l)} - \in_2^{(l)} - \omega_s^{(l)}$, where $\omega_s^{(l)}$ is the frequency of the classical control field shown in Fig. 1(a) between states $\|2\rangle \leftrightarrow \|3\rangle$ in the lth scatterer. The detuning between the mode b_l and the lth scatterer is given by $\Delta_b^{(l)} = \in_3^{(l)} - \in_1^{(l)} - \omega_b^{(l)}$. We take $\in_j^{(l)}$ to be the eigenenergy of state $\|j\rangle$ of the lth scatterer, with $j \in \{1, 2, 3\}$.
Intrinsic coupling	$\hat{H}_{\rm cc}$	Describes the intrinsic cross coupling among the cavity modes $\hat{a}$ and $\hat{b}_l$, with small rates $h_0^{(l)}$ due to, e.g., evanescent coupling and Rayleigh, Brillouin, and Raman scattering.
Scatterer coupling	$\hat{H}_{\rm sc}$	Describes the coherent coupling between the cavities modes $\hat{a}$ and $\hat{b}_l$ and scatterers via the $\|1\rangle \leftrightarrow \|3\rangle$ transition, with coupling strengths g_a and $g_b^{(l)}$.
External controls	$\hat{H}_{\rm c}$	For tuning method (A) or Stark control, we omit the classical fields required by method (B) [set $\Omega_p^{(l)}(t) = 0$] and define $\Omega_s^{(l)}(t)$ as the intense classical Stark optical fields. For tuning method (B) or shuffling control, we set both $\Omega_p^{(l)}(t)$ and $\Omega_s^{(l)}(t)$ to be nonzero and finite in amplitude and duration to form a pair of STIRAP pulses. To distinguish between the two tuning methods, we denote the control fields by $[\Omega_s^{(l)}(t)]$ for (A) Stark control and by $[\tilde{\Omega}_p^{(l)}(t), \tilde{\Omega}_s^{(l)}(t)]$ for (B) shuffling control. Each classical control field only drives one scatterer and for the Stark control has an oscillation, with the Rabi frequency $\{\omega_s^{(l)}, \Omega_s^{(l)}\}$ driving the $\|2\rangle \leftrightarrow \|3\rangle$ transition, while for the state swap, the control field has a Rabi frequency of $\{\omega_p^{(l)}, \tilde{\Omega}_p^{(l)}\}$ ($\{\omega_s^{(l)}, \tilde{\Omega}_s^{(l)}\}$), driving the $\|1\rangle \leftrightarrow \|3\rangle$ ($\|2\rangle \leftrightarrow \|3\rangle$) transition of the lth scatterer. Both $\Delta_a^{(l)}$ and $\Delta_b^{(l)}$ are assumed to be red detuned, while the control fields are blue detuned $\Delta_s^{(l)} = \in_3^{(l)} - \in_2^{(l)} - \omega_s^{(l)}$, $\Delta_p^{(l)} = \in_3^{(l)} - \in_1^{(l)} - \omega_p^{(l)}$, and $\tilde{\Delta}_p^{(l)} = \Delta_a^{(l)} + \Delta_{\rm in} - \Delta_p^{(l)}$. In this case, we can avoid generating any Raman transition involving the cavity mode when the controlling Stark or STIRAP fields are applied.

scatterer to obtain a reduced Hamiltonian $\hat{H}_{\rm red}$. This reduction is justified, as we will work far off resonance, and the excited-state population will be negligible. To do this elimination, we drop the last term $\hat{H}_{\rm c}$ in Eq. (3a) and assume that $g_a = g_b = g$ and $\omega_a = \omega_b = \omega$, $|\delta| \ll (\omega_b + \omega_a)$. Applying the rotating-wave approximation, the reduced Hamiltonian takes the following form (please refer to Appendix A for more details):

$$\hat{H}_{\rm red} = \left(\Delta_{\rm in} - \frac{|g|^2}{\Delta}\hat{\sigma}_{11}\right)\hat{a}^\dagger\hat{a} + \left(\Delta_{\rm in} - \frac{|g|^2}{\Delta}\hat{\sigma}_{11}\right)\hat{b}^\dagger\hat{b} + \left(h_0 - \frac{|g|^2}{\Delta}\hat{\sigma}_{11}\right)(\hat{b}^\dagger\hat{a} + \hat{a}^\dagger\hat{b}) + i\sqrt{2\kappa_{\rm ex}}(\alpha_{\rm in}\hat{a}^\dagger - \alpha_{\rm in}^*\hat{a}), \quad (6)$$

where we have an effective coherent coupling $\langle h_{\rm eff}\rangle = \langle h_0 - \frac{|g|^2}{\Delta}\hat{\sigma}_{11}\rangle \sim (h_0 - \frac{|g|^2}{\Delta})\langle\hat{\sigma}_{11}\rangle + h_0\langle\hat{\sigma}_{22}\rangle$. For $|\Delta|^2 \gg |g|^2\langle\hat{a}^\dagger\hat{a}\rangle$, $|g|^2\langle\hat{b}^\dagger\hat{b}\rangle$, the population in state $\|3\rangle$ is negligible. Throughout our investigation below, state $\|3\rangle$ is assumed to be adiabatically eliminated and is negligibly populated. For the sake of simplicity, we neglect the intrinsic scattering or coupling $h_0 = 0$. Thus, $h_{\rm eff} = -\frac{|g|^2}{\Delta}\sigma_{11}$. We assume the same intrinsic decay rate $\kappa_i^{(a)} = \kappa_i^{(l)} = \kappa_i$ and the same external coupling $\kappa_{\rm ex} = \kappa_{\rm ex}^{(l)}$ as well. Then, $\kappa_a = \kappa_b$. In numerical simulations, we assume $\langle\hat{O}_s\hat{O}_{a/b}\rangle \approx \langle\hat{O}_s\rangle\langle\hat{O}_{a/b}\rangle$ for a coherent input, where $\hat{O}_s$, $\hat{O}_a$, and $\hat{O}_b$ are operators related to the scatterer, mode $\hat{a}$, and mode $\hat{b}$, respectively. The resulting semiclassical equations of motion for the mean values of the observables are valid when the scatterers are weakly driven by the cavity modes and also excited by a coherent input field. This approximation has been widely used in the study of cQED systems [5,29,30].

IV. STEADY-STATE SOLUTION

We now work to obtain expressions for the transmission T_a, where light is routed out of the exit waveguide connected to cavity a, and T_b, where light is routed out of the exit waveguide connected to cavity b. Setting $h = \frac{|g|^2}{\Delta} \times \langle\hat{\sigma}_{11}\rangle$, we redefine the detuning as $\Delta'_{\rm in} = \Delta_{\rm in} - h$. We now calculate the steady-state transmission using the reduced Hamiltonian Eq. (6). We assume the maximum coupling $h_{\rm max} = 8\kappa_i$ and a minimum $h_{\rm min} = 0$, such that $0 \le h \le h_{\rm max}$. Such maximum coupling strength is easy to realize,

using the current experimental technology. Note that $h = 0$ is achievable in practice only if h_0 is zero for the shuffling control or a small h_0 is canceled by $\frac{|g|^2}{\Delta}\langle\hat{\sigma}\rangle_{11}$ in $h_{\rm eff}$ for the Stark control. In the steady state, the transmission amplitudes t_a and t_b are given by

$$t_a = \frac{\Delta'_{\rm in}(\Delta'_{\rm in} - 2i\kappa_i) + \kappa_{\rm ex}^2 - (\kappa_i^2 + h^2)}{(i\Delta'_{\rm in} + \kappa_{\rm ex} + \kappa_i)^2 + h^2}, \tag{7a}$$

$$t_b = -\frac{2ih\kappa_{\rm ex}}{(i\Delta'_{\rm in} + \kappa_{\rm ex} + \kappa_i)^2 + h^2}. \tag{7b}$$

The corresponding transmission coefficients are $T_a = |t_a|^2$ and $T_b = |t_b|^2$. When the transmission of signal is high, the state of channel is "on" and the transmission is denoted by $T_{\rm on}$. On the contrary, $T_{\rm off}$ indicates a low-level output. The performance in switching the output on or off can be evaluated using the switching contrast

$$\mathrm{SC} = (T_{\rm on} - T_{\rm off})/(T_{\rm on} + T_{\rm off}).$$

In our system, the external coupling $\kappa_{\rm ex}$ is fixed once the setup is fabricated. However, by changing the detuning Δ using a strong Stark pulse, we can change the intermode coupling strength h. As there is no fixed value for this coupling strength h, there is no fixed critical coupling $\kappa_{\rm ex}$. To demonstrate optical switching with high performance, we choose a critical coupling $\kappa_m = \sqrt{h_{\rm max}^2 + \kappa_i^2}$ for the maximum $h_{\rm max}$. The steady-state transmission coefficients $T_a = |t_a|^2$ and $T_b = |t_b|^2$ are shown in Fig. 2.

We see that in Fig. 2, as we turn on the intermode cavity coupling (solid blue to dashed red lines), the input light is blocked from exiting via the "straight-through" port a [Fig. 2(a)] and now exits via port b [Fig. 2(b)]. We also note that in comparison with the situation of critical coupling for $h = 0$, the spectral window for switching is broad and flat in our overcoupled regime, the bandwidth being determined by $h_{\rm max}$. This wide bandwidth promises a fast switching speed. For a large coupling $h = h_{\rm max}$, almost all of the input field is reflected [in the setup of Fig. 1(b)] or transmitted to another waveguide through cavity $\hat{b}$ [in the setup of Fig. 1(c)]. As seen in Fig. 2, the straight-through transmission T_a is flat and vanishing ("off" state), but T_b is large, about 0.8 (on state). On the contrary, for $h = h_{\rm min}$,

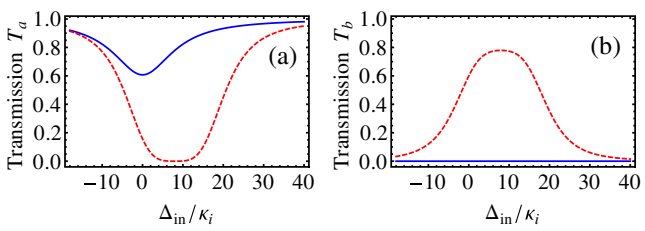

FIG. 2. Steady-state transmissions T_a and T_b as a function of detuning in the case of overcoupling. The solid blue line indicates the case for $h = 0$, the dashed red line for $h = 8\kappa_i$; $\kappa_{\rm ex} = \kappa_m$.

the incident field exits mainly from the straight-through output port $\alpha_{\rm out}$ ($T_a = 0.8$), whereas $T_b = 0$. In contrast to previous works [4,6,11], for the case of an off state in both output ports, the transmission is vanishingly small in our system. This near extinction in the off state indicates a significant advantage of our scheme: a nearly unit switching contrast.

V. TIME-DEPENDENT CONTROL

To verify our analysis and study the temporal switching behavior, we numerically solve Eq. (2). Since the population of the excited state $|3\rangle$ is negligible throughout the protocol, the decay of the scatterer is neglected, i.e., $\gamma_{31} = \gamma_{32} = 0$. Throughout the modeling below, we use $\delta = 0$, $\Delta = 800\kappa_i$, $g = 80\kappa_i$, and $h_0 = 0$, yielding an effective coherent coupling $h = 8\kappa_i$ when $\langle\sigma_{11}\rangle \sim 1$, and $\Delta_{\rm in} = 8\kappa_i$. The change in transmission due to a small static coupling, e.g., $h_0 = \kappa_i$ between cavities, is negligible, and in addition, this static coupling can be canceled via the Stark control according to Eq. (6) if $\frac{|g|^2}{\Delta}\langle\sigma_{11}\rangle = h_0$ and $\langle\sigma_{22}\rangle \sim 0$.

We take the controlling optical fields to be a train of pulses, either on Ω_s (Stark control) or pulse pairs $\tilde{\Omega}_p$ and $\tilde{\Omega}_s$ (STIRAP fields for shuffle control).

For Stark control, we choose the form of the Stark field for each pulse to be

$$\Omega_s(t) = \frac{\Omega_0}{\pi}\left[\arctan\left(\frac{t - \tau_d}{\tau}\right) - \arctan\left(\frac{t - \tau_d - \tau_w}{\tau}\right)\right],$$

where the Stark field with an amplitude of Ω_0 is blue detuned with respect to the transition $|3\rangle \leftrightarrow |3\rangle$, $\tau_{d(w)}$ is the delay (width) of the pulse, while τ is a parameter characterizing the rise or fall time of the pulse. For the Stark control protocol, we choose $\Omega_0 = 3200\kappa_i$ and $\tau = 10^{-3}\kappa_i^{-1}$. Since for Stark control the populations in states $|2\rangle$ and $|3\rangle$ are negligible, the detuning Δ_s can be much smaller than Ω_0, $\Delta_s = \Omega_0/10$, in order to provide a large Stark shift $\Omega_0^2/\Delta_s = 3.2 \times 10^4\kappa_i$.

For shuffle control, we use the technology of STIRAP, which is robust against noise in the fields to swap the group-state internal populations of the scatterer. To avoid the disturbance from the cavity modes, the fields are blue detuned again but on a two-photon resonance. The STIRAP pulses $\tilde{\Omega}_p$ and $\tilde{\Omega}_s$ have the same profile as the above-mentioned Stark control pulse but have different widths and delays and are given by

$$\tilde{\Omega}_{p,s}(t) = \Omega'_0 e^{-(t-\tau_{p,s})^4/2\tau_w^2},$$

where Ω'_0 is the amplitude, τ_w characterizes the width of the pulses, and $\tau_{p,s}$ the delay. Control fields with $\tau_w = 10^{-3}\kappa_i^{-1}$, which operate much faster than the ring-down time of the cavity, effect a nearly instantaneous turning on or off of the intermode coupling.

A. All-optical switching

First, we demonstrate all-optical switching of the transmission T_a in the two schemes: (A) Stark control and (B) shuffle control. We take the initial state of the scatterer to be $|1\rangle$, i.e., $\langle\sigma_{11}\rangle = 1$. Referring to the numerical results shown in Fig. 3, both schemes yield a short initial burst in transmission that is due to a short starting process of the system $\kappa_i t < 0.2$. Because the cavity is empty, the forward transmission T_a is large during this period, according to the input-ouput relation Eq. (5). To demonstrate an example of switching behavior, we consider the output when $\kappa_i t \geq 1$. From the results shown in Fig. 3, we observe that the output closely follows the controlling Stark field [see the dashed blue line in Fig. 3(a)], while the STIRAP control toggles the output in Fig. 3(b) (see the solid blue lines). The $1/e$ switching time is short, about $0.1\kappa_i^{-1}$, and the transmission remains constant, 0.8, for both schemes in the steady state. These numerical results agree closely with our analysis given in Eq. (7) and Fig. 2.

In the Stark control protocol, a Stark field $\Omega_s(t)$ is used to switch on or off the induced coherent coupling between cavity modes $\hat{a}$ and $\hat{b}$. The amplitude Ω_0 of the applied Stark field is $3200\kappa_i$. This value can be reduced if the detuning Δ_s is reduced. If the intrinsic quality factor Q_0 of the cavity exceeds $\sim 10^6$, corresponding to a total quality factor $Q > 10^5$ because of the overcoupling to waveguides, then the coupling strength and control pulse can be reduced, $g < 10$ GHz and $\Omega_0 < 320$ GHz corresponding to an intensity of $I \sim 2 \times 10^5$ W/cm^2 if the dipole moment of the scatterer is typically $\vec{d} \sim 3 \times 10^{-29}$ C $\cdot$ m. For $\Omega_s = 0$, the coherent interaction h is maximum $h_{\max}$. As a result, the straight-through output is off and the transmission $T_a \approx 0$. When Ω_s is applied, the induced Stark shift is large enough to switch off h. This vanishingly small $h_{\min}$ leads to $T_a = 0.8$ when the system reaches the steady state. Our numerical simulations show that the transmission T_a can be turned off at its peaks before it reaches the steady states. Thus, one can encode information more densely within the same duration.

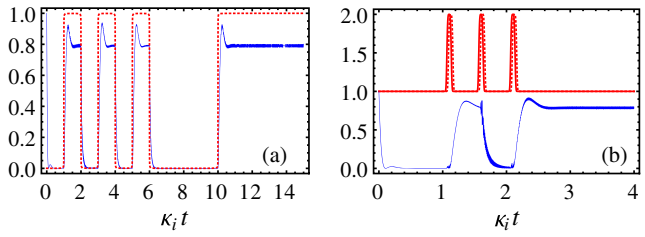

FIG. 3. All-optical switching controlled via (A) Stark control and (B) shuffle control. The dashed red lines indicate the normalized controlling fields [Stark field for (A) and STIRAP field for (B)]. The STIRAP fields are offset for clarity. The solid blue line represents the transmission T_a. $\Delta_s = -320\kappa_i$ and $\Omega_0 = 10\Delta_s$ for (a), and $\Delta_p = \Delta_s = -200\kappa_i$, $\Omega_0' = 100\kappa_i$, and $\tau_s - \tau_p = 0.025\kappa_i^{-1}$ for (b). The switching time is about $0.1\kappa_i^{-1}$. In (A), we observe that the straight-through transmission closely follows the Stark pulse, while in (B), we see that this transmission is toggled on and off by the shuffle control pulses.

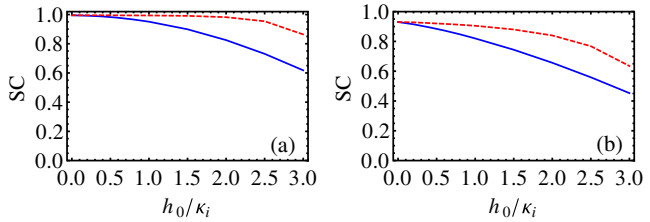

FIG. 4. Switching contrast as a function of the intrinsic coupling for (a) Stark control and (b) shuffle control. The time averages of transmissions T_{on} and T_{off} in Fig. 3 are used. T_{on} is evaluated over the time period from $\kappa_i t = 1.5$ to 2 in (a) and from $\kappa_i t = 1.4$ to 1.6 in (b), while T_{off} is calculated from $\kappa_i t = 2.5$ to 3 in (a) and from $\kappa_i t = 1.8$ to 2 in (b). The solid blue lines indicate the fixed external coupling $\kappa_{\text{ex}} = \sqrt{h_{\max}^2 + \kappa_i^2}$, while the dashed red lines present the optimal critical coupling $\kappa_{\text{ex}} = \sqrt{(h_{\max} - h_0)^2 + \kappa_i^2}$ and $\Delta_{\text{in}} = h_{\max} - h_0$.

In the shuffle control protocol, the STIRAP pulse fields are used to swap the internal population of the scatterer between states $|1\rangle$ and $|2\rangle$. The scatterer is initially prepared in $|1\rangle$, i.e., $\langle\hat{\sigma}_{11}\rangle = 1$, and the transmission T_a is negligible. When the population is swept to $|2\rangle$, the coherent coupling h vanishes because of $\langle\hat{\sigma}_{11}\rangle = 0$, and subsequently the system yields a large straight-through transmission $T_a = 0.8$. Each pair of STIRAP fields encodes 1 bit of information into the output α_{out} and toggles the output on and off. In comparison with the Stark control protocol, an important advantage of the shuffle control protocol is that the applied classical control fields are much weaker, about $\Omega_0' = 100\kappa_i$.

It is important in practice to look into the performance of devices under the situation of nonzero intrinsic coupling h_0. The switching contrast is used in Fig. 4 to show the robustness of our devices against small h_0. It can be seen that the switching contrast decreases slowly as h_0 increases. For a reasonably small coupling $h_0 < 2\kappa_i$, SC > 0.8 for the Stark control and SC $> 2/3$ for the shuffling control. If we apply an optimal control scheme (dashed red lines), $\kappa_{\text{ex}} = \sqrt{(h_{\max} - h_0)^2 + \kappa_i^2}$ and $\Delta_{\text{in}} = h_{\max} - h_0$, then the switching contrast can be larger than 0.8 for two protocols.

B. All-optical router

Using our routing concepts, we can control not only the forward transmission but also the output β_{out} from the waveguide coupled to the cavity mode $\hat{b}$, as shown in Fig. 2(b). In contrast to previously published works, our scheme can route photons to many different output ports. One possible setup for an all-optical router is illustrated in Fig. 1(d). Here, the photons can be selectively sent out to ports α_{out} or $\beta_{\text{out}}^{(l)}$. Unlike Ref. [9], which demultiplexed

the total field energy into several ports and then controlled the output of each port, each output port in our scheme withdraws light separately from a common cavity. So, the switching fidelity of each output in our setup is independent of the number of ports.

To illustrate this independence, we refer the reader back to the router schematic setup with two possible output ports in addition to the straight-through port, as illustrated in Fig. 1(d). This arrangement now uses two scatterers, one common cavity $\hat{a}$, and two coupled cavities $\hat{b}_1$ and $\hat{b}_2$. Following numerical modeling, we depict the operation of this dual-output all-optical router in Fig. 5 with output ports $\beta_{\rm out}^{(1)}$ (solid blue line) and $\beta_{\rm out}^{(2)}$ (dashed red line) either controlled by the Stark tuning [Figs. 5(a) and 5(b)] or via shuffling tuning [Figs. 5(c) and 5(d)]. We switch off the output $\alpha_{\rm out}$ due to the large h_l when tuning on the coupling to ports $\beta_{\rm out}^{(l)}$. The profiles of controlling laser pulses are the same as in Fig. 3, but the delays are different. The scatterers are individually controlled by the corresponding laser pulse trains. In the Stark control, scatterers always stay in state $|1\rangle$, i.e., $\langle\sigma_{11}\rangle = 1$, but strong Stark fields are applied to eliminate the effective coupling h. In the shuffling control, all scatterers are initially populated in state $|2\rangle$. Thus, the ports $\beta_{\rm out}^{(l)}$ are initially isolated from the input field. As a result, all β ports are initially off. The coupling h for each scatterer is sequentially switched on, to $h_{\rm max}$, when the Stark field is turned off [see Fig. 5(a)] (Stark control) or the scatterer is swept into state $|1\rangle$ [see Fig. 5(c)] (shuffling control). Therefore, the input field is routed to either waveguide β_1 ($T_1 \approx 0.8$) or β_2 ($T_2 \approx 0.8$), which means that either output turns on. As shown in Figs. 5(b) and 5(d), the binary optical information "1010" and "0101" is encoded into ports $\beta_{\rm out}^{(1)}$ and $\beta_{\rm out}^{(2)}$, respectively.

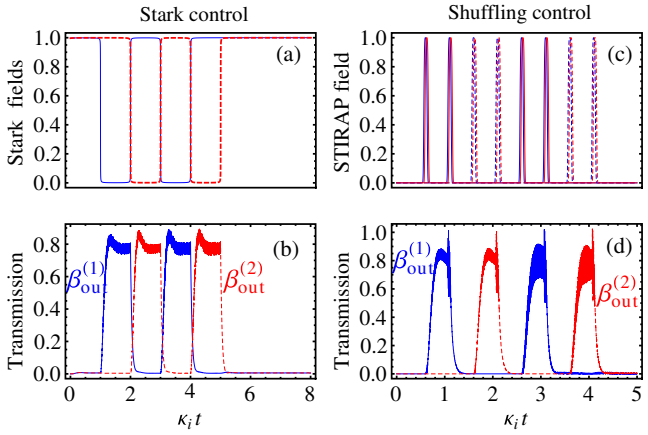

FIG. 5. All-optical routing in output channels (a),(b) Stark control and (c),(d) shuffling control. Parts (b) and (d) show the light in the output channels and prove that one can reroute the light into the two separate output channels with a near-perfect contrast (bright and dark). Parts (a) and (c) depict the Stark and STIRAP classical control pulses used. Initially, $\langle\hat{\sigma}_{11}(0)\rangle = 1$ in Stark control protocol but $\langle\sigma_{22}(0)\rangle = 1$ in shuffling control. The parameters and the profiles for the control fields $\tilde{\Omega}_p^{(l)}$ and $\tilde{\Omega}_s^{(l)}$ are the same as in Fig. 3. The solid and dashed lines in (a) and (c) indicate the field applied to control scatterers 1 and 2, respectively. The solid blue lines in (b) and (d) are for the output $\beta_{\rm out}^{(1)}$, but the dashed red lines are for $\beta_{\rm out}^{(2)}$. The blue lines in (c) represent the field $\tilde{\Omega}_p^{(l)}$; the red lines are $\tilde{\Omega}_s^{(l)}$.

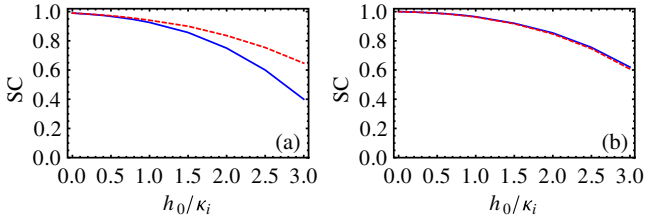

FIG. 6. Switching contrast as a function of the intrinsic coupling for (a) Stark control and (b) shuffle control. The solid blue lines indicate the output $\beta_{\rm out}^{(1)}$, while the dashed red lines are for the output $\beta_{\rm out}^{(2)}$. The time averages of $T_{\rm on}$ and $T_{\rm off}$ in Fig. 5 are used to evaluate the switching contrast. In (a), $T_{\rm on}$ is evaluated from $\kappa_i t = 1.5$ to 2 for $\beta_{\rm out}^{(1)}$ and from $\kappa_i t = 2.5$ to 3 for $\beta_{\rm out}^{(2)}$; $T_{\rm off}$ is calculated from $\kappa_i t = 2.5$ to 3 for $\beta_{\rm out}^{(1)}$ and from $\kappa_i t = 3.5$ to 4 for $\beta_{\rm out}^{(2)}$. In (b), $T_{\rm on}$ is the average transmission between $\kappa_i t = 0.8$ and 1.1 for $\beta_{\rm out}^{(1)}$ and between $\kappa_i t = 1.8$ and 2.1 for $\beta_{\rm out}^{(2)}$; $T_{\rm off}$ is averaged over the time period from $\kappa_i t = 1.5$ to 2 for $\beta_{\rm out}^{(1)}$ and from $\kappa_i t = 2.5$ to 3 for $\beta_{\rm out}^{(2)}$. The fixed external coupling $\kappa_{\rm ex} = \sqrt{h_{\rm max}^2 + k_i^2}$ is applied in all cases.

Unlike the demultiplexer-type router [9], the output of each port is similar because the energy of the input light is only transferred to the port that is switched on. This setup promises a small insertion loss of 20% independent of the number of output ports. If two output ports simultaneously turn on, the light energy will be evenly fed into two ports.

Our optical routers are also robust against the small h_0, as shown in Fig. 6. The outputs $\beta_{\rm out}^{(1)}$ and $\beta_{\rm out}^{(2)}$ decrease slightly in both protocols. For example, for $h_0 = 2\kappa_i$, the switching contrast of $\beta_{\rm out}^{(2)}$ is still 0.84, and that of $\beta_{\rm out}^{(1)}$ slightly decreases to 0.75 in the Stark control, while it can remain 0.85 in the shuffling control. Such a level of switching contrast allows for routing quality larger than 0.75 in optical communications up to an intrinsic coupling of $h_0 = 2\kappa_i$.

VI. DISCUSSION OF IMPLEMENTATION

The implementation of our scheme requires a strong coupling between a three-level Λ-type solid-state quantum system and a single photon in a "good" optical cavity. A coupling strength of GHz is already available in quantum-dot–cavity systems [4,31,32], in NV center-cavity systems [33], and in Bose-Einstein condensate-cavity systems [34]. The deep strong-coupling regime of $g = 80\kappa_i$ requires that the cavity has an intrinsic quality factor $Q_0 > 10^6$ but a total quality factor $Q > 10^5$. This requisite can be met using either photonic crystal cavities [9,35–37] or toroidal cavities [38,39]. If the state-of-the-art technique can

combine strong coupling [31] and a high-Q cavity [38], the rate g/κ_i can reach 10^4 [40]. The Λ-type scatterer can be a single NV center in nanodiamond at low temperature [41–43], quantum dot [44], or rare-earth ion-doped crystals [45,46]. Therefore, our scheme for all-optical switching or routing can be realized on a chip in various kinds of systems using current experimental techniques.

Another important requisite is to effectively couple the scatterer to two cavities simultaneously but greatly suppress the intrinsic coupling or the natural cross-talk coupling between the modes (coupling without the scatterer present). This issue has been solved in recent state-of-the-art experiments. If we consider the two degenerate modes to be counterpropagating modes in a toroidal cavity, many groups can make toroidal cavities with a negligible intrinsic scattering ($2h_0 < \kappa_i + \kappa_{ex}$) using existing technology [38,39,47]. If one now inserts quantum dots or nanodiamonds into a cavity, their geometric profiles cause additional scattering or cross talk between modes in the cavity. This cross talk is unwanted—we only wish to have cross coupling mediated by the dipole coupling to the internal states of the scatterer. The geometrical scattering rate caused by a nanoparticle decreases quickly ($\propto r^3$) as the size (radius r) of particle decreases [10]. Therefore, the effects of geometric scattering can be neglected for a scatterer with $r < 10$ nm. Experiments have demonstrated that the scattering of a toroidal cavity embedding a nanoparticle only causes negligible broadening of the linewidth of the cavity mode, even with a Q factor $Q > 10^8$ [38] much larger than that which we require.

Rather than use degenerate modes in a toroidal cavity, one instead seeks to use two spatially separated cavities, e.g., two photonic crystal cavities, and one can also decouple these cavities from each other if their mode fields are orthogonally polarized in the $\hat{E}_x$ and $\hat{E}_y$ in planes [48], respectively. In Ref. [48], the authors have demonstrated experimentally spatially overlapping one-dimensional (1D) photonic crystal cavities that are individually tunable and that are engineered to have very little cross-talk coupling. In this arrangement, by positioning the scatterer at the spatial crossing point of the two 1D photonic crystal (PC) cavities and arranging that the dipole moment of the nanoscatterer is oriented along the direction of $\hat{E}_x + \hat{E}_y$, one can couple the scatterer to each cavity mode with little intrinsic cross talk between the cavity modes. This configuration of orthogonal polarized cavities can be extended for our multiport optical routers (see Appendix B).

Now, we estimate the energy cost of our setup. Assuming a typical transition dipole moment of $\vec{d} = 3.0 \times 10^{-29}$ C · m and a refractive index of $n \sim 3$, the required electric field E is about 10^5 V/m, which corresponds to an intensity of $I = 2 \times 10^5$ W/cm^2 required to achieve the strong Stark field $\Omega_0 = 320$ GHz. Because of the large dipole moment [49], the intensity required to drive a quantum dot can be lower [44]. Classical binary information can be encoded at 100-MHz rates. To neglect the creation of any cavity excitations, the Stark pulse energy can be as low as 2 pJ/bit if the field is tightly focused to 1 μm^2. Optical control of nanoscale scatterers like NV centers or quantum dots can also avoid exciting the optical cavity. Therefore, the required energy cost can be reduced to 24 fJ/bit if we focus the fields into a nanosized area 15×80 nm^2 using plasmons [50–52]. If we drive the scatterers via the excitation of another cavity mode [4], the laser power incident into the waveguide can be 50 nW (refer to the Supplemental Material of Ref. [4]). This energy cost is comparable to recent work using InGaAsP materials [9]. More interestingly, our second proposed scheme, involving shuffle control, where one routes photons via the coherent control of the ground-state populations, requires vastly lower control powers than the Stark control scheme. The intensity ($I \sim 200$ W/cm^2) of the STIRAP fields can be three orders lower than the intensity required for the Stark fields ($\Omega_0 = 3200\kappa_i$), thus indicating that the shuffle protocol will be far more economical to control from a practical viewpoint.

VII. CONCLUSION

In conclusion, we present a protocol to dynamically control the coupling between two cavity modes. Using this protocol, all-optical switching and routing are demonstrated using numerical simulations. The wide bandwidth of transmission promises a short switching time and dense encoding capability. Because the photonic output while in the off state vanishes, a unit switching contrast is obtained. The output of the router is high and independent of the number of ports. If two scatterers are entangled in their ground states, our proposal will be able to create entangled coherent output fields.

APPENDIX A: DERIVATION OF THE REDUCED HAMILTONIAN $\hat{H}_{red}$ IN EQ. (6)

Here, we provide greater detail regarding the intermediate steps to obtain Eq. (6) from Eq. (3) in the main text. We enable optical routing by modulating the coupling strength between two cavity modes, thus allowing the directed transmission of an incoming signal through the coupled-cavity system and out to an exit waveguide. To study the routing, we only need to consider one switching or routing node that consists of two cavity modes, the atomic scatterer, the input signal, and the associated classical control fields. The control fields serve to control the dynamics of the scattering either via (a) Stark tuning via a rapid tuning of the transition energy of the scatterer through the application of an intense Stark pulse or via (b) shuffling by turning on or off the intercavity coupling by transferring the scatterer's internal atomic state to an internal state that does not couple to either cavity.

In our setup, depicted in Fig. 1(a), the arrangements of classical and quantum fields are far from two-photon resonance, and thus any Raman transitions induced by these fields between the two ground states of the scatterer are greatly suppressed. Thus, we can neglect the term $\hat{H}_c$ in Eq. (3f) (due only to the classical control fields). As we are only considering a single node, we drop the index $(l)(l = 1)$ in Eq. (3) and replace $(\Delta_a^{(l)}, \Delta_s^{(l)}, \delta_l, h_0^{(l)}, g_b^{(l)}, \hat{b}_l, \sigma_{11}^{(l)}, \sigma_{22}^{(l)}, \sigma_{13}^{(l)})$ by $(\Delta_a, \Delta_s, \delta, h_0, g_b, \hat{b}, \sigma_{11}, \sigma_{22}, \sigma_{13})$.

To proceed, we assume that $g_a = g_b = g$ and that $\omega_a = \omega_b$, which gives $\delta = 0$. In the dispersive coupling regime, the population of the excited state $|3\rangle$ is negligible. We can therefore adiabatically eliminate this excited state from the original Hamiltonian $\hat{H}' = \hat{H} - \hat{H}_c$ and derive an effective reduced Hamiltonian $\hat{H}_{red}$. $\hat{H}$ and $\hat{H}_c$ are given by Eq. (3). Using $\frac{\partial Q}{\partial t} = i[\hat{H}', Q]$ and applying the rotating-wave approximation, we obtain

$$\dot{\hat{\sigma}}_{13} = -i(\Delta + \Delta_{in})\hat{\sigma}_{13} + ig(\hat{\sigma}_{33} - \hat{\sigma}_{11})(\hat{a} + \hat{b}).$$

Note that the detuning Δ_{in} is introduced because of the external driving of the cavity, which is independent of the scatterer. This detuning causes the operators $(\hat{\sigma}_{13}, \hat{a}, \hat{b})$ to oscillate at frequency Δ_{in}. The oscillation can be eliminated from the equation by replacing $(\hat{\sigma}_{13}, \hat{a}, \hat{b})$ by $(e^{-i\Delta_{in}t}\hat{\tilde{\sigma}}_{13}, e^{-i\Delta_{in}t}\hat{\tilde{a}}, e^{-i\Delta_{in}t}\hat{\tilde{b}})$.

Since $\langle\hat{\tilde{\sigma}}_{13}\rangle$ varies slowly and the population in $|3\rangle$ is small, it is reasonable to assume $\dot{\hat{\sigma}}_{13} \sim 0$ [53–55]. This assumption gives

$$\hat{\sigma}_{13} \approx \frac{g}{\Delta}(\hat{\sigma}_{33} - \hat{\sigma}_{11})(\hat{a} + \hat{b}). \tag{A1}$$

Substituting Eq. (A1) into the cavity-scatterer interaction Hamiltonian $\hat{H}_{sc}$ (3e), we obtain

$$\hat{H}'_{sc} \approx -\frac{|g|^2}{\Delta}\hat{\sigma}_{11}(\hat{a}^\dagger\hat{a} + \hat{b}^\dagger\hat{b}) - \frac{|g|^2}{\Delta}\hat{\sigma}_{11}(\hat{a}^\dagger\hat{b} + \hat{b}^\dagger\hat{a}). \tag{A2}$$

Here, we have dropped the terms from $\hat{H}_0$ that only associate with $\hat{\sigma}_{11}$ or $\hat{\sigma}_{22}$, which commute with $\hat{H}_{red}$, and also drop the terms associated with small $\hat{\sigma}_{33}$. We also correct the effective Hamiltonian $\hat{H}'_{sc}$ by dividing by 2. The necessity of this renormalization is verified by numerically comparing the Raman transition of a full three-level Λ-type system and its effective two-level counterpart when the excited state is eliminated. This correction has also been justified by other works [54,55]. After substituting Eq. (A2) into Eq. (3), the reduced Hamiltonian given by Eq. (6) is obtained.

APPENDIX B: IMPLEMENTATION OF OPTICAL ROUTERS

Here, we present a configuration for the optical router with one forward input-output port and two cross output ports. This configuration uses either the 1D nanobeams [48] or 1D or 2D PC cavities [56,57] in a planar configuration. The possible realizations of a three-port optical router are shown in Figs. 7(a) and 7(b). These designs are used to show the main idea of how to suppress the intrinsic coupling between cavities and allow one to construct multiport devices, but are not meant to be a detailed study of the optimal configuration.

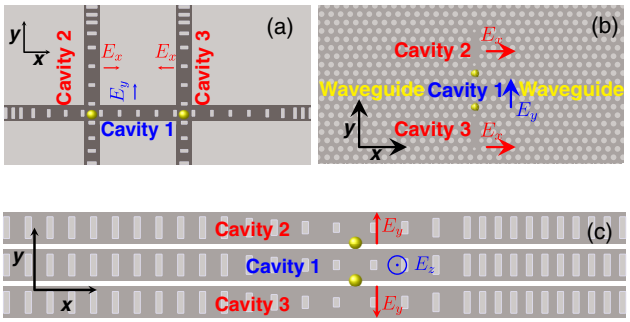

FIG. 7. Possible construction of multiport optical routers. (a) Realization using nanobeam cavities. (b) Realization using PC cavities. (c) Realization using side-by-side layout nanobeams.

We suggest three structures for our multiport optical router. The light is always incident into cavity 1 and is routed into the β output ports [not shown in Fig. 7(b)] mediated by the associated cavities 2 and 3. The polarization of the electric field of a cavity mode is perpendicular to the 1D cavity axis [48,56–60]. Therefore, one can engineer the orientation of the polarization of the cavity mode. In structures (a) and (b), cavity 1 is y polarized, but the other two cavities are polarized along x axis. In this configuration, cavities 1, 2, and 3 decouple from each other, and their couplings can be only mediated by the scatterers. Unlike structures (a) or (b), in the side-by-side configuration (c) [61], cavity 1 can be z polarized if it is thick in the z direction [58,60], while cavities 2 and 3 are y polarized. There, three arrangements can suppress the intrinsic coupling between cavities but allow interactions that are only mediated by the scatterers. Since the mode volume of a nanobeam nanocavity or a PC nanocavity is very small, the cavity-scatterer interaction can still be strong enough, even if two nanocavities (e.g., cavity 1 and cavity 2 or 3) is spatially separated. So, our multiport optical router can be experimentally realized using the geometry structures shown in Fig. 7.

[1] Q. Xu, P. Dong, and M. Lipson, *Breaking the Delay-Bandwidth Limit in a Photonic Structure*, Nat. Phys. **3**, 406 (2007).

[2] C. Zheng, X. Jiang, S. Hua, L. Chang, G. Li, H. Fan, and M. Xiao, *Controllable Optical Analog to Electromagnetically Induced Transparency in Coupled*

High-Q Microtoroid Cavities, Opt. Express **20**, 18319 (2012).

[3] K. Totsuka, N. Kobayashi, and M. Tomita, *Slow Light in Coupled-Resonator-Induced Transparency*, Phys. Rev. Lett. **98**, 213904 (2007).

[4] R. Bose, D. Sridharan, H. Kim, G. S. Solomon, and E. Waks, *Low-Photon-Number Optical Switching with a Single Quantum Dot Coupled to a Photonic Crystal Cavity*, Phys. Rev. Lett. **108**, 227402 (2012).

[5] B. Dayan, A. S. Parkins, T. Aoki, E. P. Ostby, K. J. Vahala, and H. J. Kimble, *A Photon Turnstile Dynamically Regulated by One Atom*, Science **319**, 1062 (2008).

[6] T. Aoki, A. S. Parkins, D. J. Alton, C. A. Regal, B. Dayan, E. Ostby, K. J. Vahala, and H. J. Kimble, *Efficient Routing of Single Photons by One Atom and a Microtoroidal Cavity*, Phys. Rev. Lett. **102**, 083601 (2009).

[7] V. R. Almeida, C. A. Barrios, R. R. Panepucci, M. Lipson, M. A. Foster, D. G. Ouzounov, and A. L. Gaeta, *All-Optical Switching on a Silicon Chip*, Opt. Lett. **29**, 2867 (2004).

[8] Y. Sato, Y. Tanaka, J. Upham, Y. Takahashi, T. Asano, and S. Noda, *Strong Coupling between Distant Photonic Nanocavities and Its Dynamic Control*, Nat. Photonics **6**, 56 (2012).

[9] K. Nozaki, A. Shinya, S. Matsuo, Y. Suzaki, T. Segawa, T. Sato, Y. Kawaguchi, R. Takahashi, and M. Notomi, *Ultralow-Power All-Optical RAM Based on Nanocavities*, Nat. Photonics **6**, 248 (2012).

[10] A. Mazzei, S. Götzinger, L. de S. Menezes, G. Zumofen, O. Benson, and V. Sandoghdar, *Controlled Coupling of Counterpropagating Whispering-Gallery Modes by a Single Rayleigh Scatterer: A Classical Problem in a Quantum Optical Light*, Phys. Rev. Lett. **99**, 173603 (2007).

[11] D. Englund, A. Majumdar, M. Bajcsy, A. Faraon, P. Petroff, and J. Vučković, *Ultrafast Photon-Photon Interaction in a Strongly Coupled Quantum Dot-Cavity System*, Phys. Rev. Lett. **108**, 093604 (2012).

[12] T. Volz, A. Reinhard, M. Winger, A. Badolato, K. J. Hennessy, E. L. Hu, and A. Imamoğlu, *Ultrafast All-Optical Switching by Single Photons*, Nat. Photonics **6**, 605 (2012).

[13] K. Nozaki, T. Tanabe, A. Shinya, S. Matsuo, T. Sato, H. Taniyama, and M. Notomi, *Sub-femtojoule All-Optical Switching Using a Photonic-Crystal Nanocavity*, Nat. Photonics **4**, 477 (2010).

[14] X. Hu, P. Jiang, C. Ding, H. Yang, and Q. Gong, *Picosecond and Low-Power All-Optical Switching Based on an Organic Photonic-Bandgap Microcavity*, Nat. Photonics **2**, 185 (2008).

[15] R. Keil, M. Heinrich, F. Dreisow, T. Pertsch, A. Tünnermann, S. Nolte, D. N. Christodoulides, and A. Szameit, *All-Optical Routing and Switching for Three-Dimensional Photonic Circuitry*, Sci. Rep. **1**, 94 (2011).

[16] B. Chen, J.-J. Li, C. Jiang, and K.-D. Zhu, *Single Photon Router in the Optical Regime Based on a Cavity Optomechanical System with a Bose-Einstein Condensate*, IEEE Photonics Technol. Lett. **24**, 766 (2012).

[17] J. T. Shen and S. Fan, *Coherent Photon Transport from Spontaneous Emission in One-Dimensional Waveguides*, Opt. Lett. **30**, 2001 (2005).

[18] M. Cheng, Y.-Q. Luo, Y.-Y. Song, and G.-X. Zhao, *Single-Photon Scattering by a Λ-Type Three-Level in a Cavity Coupling to One-Dimensional Waveguide*, Opt. Commun. **283**, 3721 (2010).

[19] D. E. Chang, A. S. Sørensen, E. A. Demler, and M. D. Lukin, *A Single-Photon Transistor Using Nanoscale Surface Plasmons*, Nat. Phys. **3**, 807 (2007).

[20] D. Witthaut and A. S. Sørensen, *Photon Scattering by a Three-Level Emitter in a One-Dimensional Waveguide*, New J. Phys. **12**, 043052 (2010).

[21] A. D. Boozer, A. Boca, R. Miller, T. E. Northup, and H. J. Kimble, *Reversible State Transfer between Light and a Single Trapped Atom*, Phys. Rev. Lett. **98**, 193601 (2007).

[22] X.-s. Li, D. L. Lin, and C.-d. Gong, *Nonresonant Interaction of a Three-Level Atom with Cavity Fields. I. General Formalism and Level Occupation Probabilities*, Phys. Rev. A **36**, 5209 (1987).

[23] Z.-d. Liu, X.-s. Li, and D. L. Lin, *Nonresonant Interaction of a Three-Level Atom with Cavity Fields. II. Coherent Properties of the Stimulated Fields*, Phys. Rev. A **36**, 5220 (1987).

[24] N. V. Vitanov, T. Halfmann, B. W. Shore, and K. Bergmann, *Laser-Induced Population Transfer by Adiabatic Passage Techniques*, Annu. Rev. Phys. Chem. **52**, 763 (2001).

[25] A. Faraon, E. Waks, D. Englund, I. Fushman, and J. Vučković, *Efficient Photonic Crystal Cavity-Waveguide Couplers*, Appl. Phys. Lett. **90**, 073102 (2007).

[26] J. Chan, T. P. Mayer Alegre, A. H. Safavi-Naeini, J. T. Hill, A. Krause, S. Gröblacher, M. Aspelmeyer, and O. Painter, *Laser Cooling of a Nanomechanical Oscillator into Its Quantum Ground State*, Nature (London) **478**, 89 (2011).

[27] M. J. Collett and C. W. Gardiner, *Squeezing of Intracavity and Traveling-Wave Light Fields Produced in Parametric Amplification*, Phys. Rev. A **30**, 1386 (1984).

[28] C. W. Gardiner and M. J. Collett, *Input and Output in Damped Quantum Systems: Quantum Stochastic Differential Equations and the Master Equation*, Phys. Rev. A **31**, 3761 (1985).

[29] R. J. Brecha, L. A. Orozco, M. G. Raizen, M. Xiao, and H. J. Kimble, *Observation of Oscillatory Energy Exchange in a Coupled-Atom–Cavity System*, J. Opt. Soc. Am. B **12**, 2329 (1995).

[30] M. Albert, J. P. Marler, P. F. Herskind, A. Dantan, and M. Drewsen, *Collective Strong Coupling between Ion Coulomb Crystals and an Optical Cavity Field: Theory and Experiment*, Phys. Rev. A **85**, 023818 (2012).

[31] K. Srinivasan and O. Painter, *Linear and Nonlinear Optical Spectroscopy of a Strongly Coupled Microdisk–Quantum Dot System*, Nature (London) **450**, 862 (2007).

[32] K. Hennessy, A. Badolato, M. Winger, D. Gerace, M. Atatüre, S. Gulde, S. Fält, E. L. Hu, and A. Imamoğlu, *Quantum Nature of a Strongly Coupled Single Quantum Dot–Cavity System*, Nature (London) **445**, 896 (2007).

[33] P. E. Barclay, C. Santori, K.-M. Fu, R. G. Beausoleil, and O. Painter, *Coherent Interference Effects in a*

Nano-assembled Diamond NV Center Cavity-QED System, Opt. Express **17**, 8081 (2009).

[34] Y. Colombe, T. Steinmetz, G. Dubois, F. Linke, D. Hunger, and J. Reichel, *Strong Atom-Field Coupling for Bose-Einstein Condensates in an Optical Cavity on a Chip*, Nature (London) **450**, 272 (2007).

[35] M. Notomi and H. Taniyama, *On-Demand Ultrahigh-Q Cavity Formation and Photon Pinning via Dynamic Waveguide Tuning*, Opt. Express **16**, 18657 (2008).

[36] P. B. Deotare, M. W. McCutcheon, I. W. Frank, M. Khan, and M. Lončar, *High Quality Factor Photonic Crystal Nanobeam Cavities*, Appl. Phys. Lett. **94**, 121106 (2009).

[37] Q. Quan and M. Loncar, *Deterministic Design of Wavelength Scale, Ultra-high Q Photonic Crystal Nanobeam Cavities*, Opt. Express **19**, 18529 (2011).

[38] I. S. Grudinin, V. S. Ilchenko, and L. Maleki, *Ultrahigh Optical Q Factors of Crystalline Resonators in the Linear Regime*, Phys. Rev. A **74**, 063806 (2006).

[39] A. Schliesser, R. Rivière, G. Anetsberger, O. Arcizet, and T. J. Kippenberg, *Resolved-Sideband Cooling of a Micromechanical Oscillator*, Nat. Phys. **4**, 415 (2008).

[40] H. Mabuchi and H. J. Kimble, *Atom Galleries for Whispering Atoms: Binding Atoms in Stable Orbits around an Optical Resonator*, Opt. Lett. **19**, 749 (1994).

[41] C. Santori, P. Tamarat, P. Neumann, J. Wrachtrup, D. Fattal, R. G. Beausoleil, J. Rabeau, P. Olivero, A. D. Greentree, S. Prawer, F. Jelezko, and P. Hemmer, *Coherent Population Trapping of Single Spins in Diamond under Optical Excitation*, Phys. Rev. Lett. **97**, 247401 (2006).

[42] P. R. Hemmer, A. V. Turukhin, M. S. Shahriar, and J. A. Musser, *Raman-Excited Spin Coherences in Nitrogen-Vacancy Color Centers in Diamond*, Opt. Lett. **26**, 361 (2001).

[43] W. L. Yang, Z. Q. Yin, Z. Y. Xu, M. Feng, and J. F. Du, *One-Step Implementation of Multiqubit Conditional Phase Gating with Nitrogen-Vacancy Centers Coupled to a High-Q Silica Microsphere Cavity*, Appl. Phys. Lett. **96**, 241113 (2010).

[44] X. Xu, B. Sun, P. R. Berman, D. G. Steel, A. S. Bracker, D. Gammon, and L. J. Sham, *Coherent Population Trapping of an Electron Spin in a Single Negatively Charged Quantum Dot*, Nat. Phys. **4**, 692 (2008).

[45] Z.-Q. Zhou, W.-B. Lin, M. Yang, C.-F. Li, and G.-C. Guo, *Realization of Reliable Solid-State Quantum Memory for Photonic Polarization Qubit*, Phys. Rev. Lett. **108**, 190505 (2012).

[46] R. Kolesov, *Coherent Population Trapping in a Crystalline Solid at Room Temperature*, Phys. Rev. A **72**, 051801(R) (2005).

[47] H. Lee, T. Chen, J. Li, K. Y. Yang, S. Jeon, O. Painter, and K. J. Vahala, *Chemically Etched Ultrahigh-Q Wedge-Resonator on a Silicon Chip*, Nat. Photonics **6**, 369 (2012).

[48] K. Rivoire, S. Buckley, and J. Vučković, *Multiply Resonant Photonic Crystal Nanocavities for Nonlinear Frequency Conversion*, Opt. Express **19**, 22198 (2011).

[49] P. G. Eliseev, H. Li, A. Stintz, G. T. Liu, T. C. Newell, K. J. Malloy, and L. F. Lester, *Transition Dipole Moment of InAs/InGaAs Quantum Dots from Experiments on Ultralow-Threshold Laser Diodes*, Appl. Phys. Lett. **77**, 262 (2000).

[50] H. Choo, M.-K. Kim, M. Staffaroni, T. J. Seok, J. Bokor, S. Cabrini, P. J. Schuck, M. C. Wu, and E. Yablonovitch, *Nanofocusing in a Metal-Insulator-Metal Gap Plasmon Waveguide with a Three-Dimensional Linear Taper*, Nat. Photonics **6**, 838 (2012).

[51] M. I. Stockman, *Nanofocusing of Optical Energy in Tapered Plasmonic Waveguides*, Phys. Rev. Lett. **93**, 137404 (2004).

[52] N. C. Lindquist, P. Nagpal, A. Lesuffleur, D. J. Norris, and S.-H. Oh, *Three-Dimensional Plasmonic Nanofocusing*, Nano Lett. **10**, 1369 (2010).

[53] C. C. Gerry and J. H. Eberly, *Dynamics of a Raman Coupled Model Interacting with Two Quantized Cavity Fields*, Phys. Rev. A **42**, 6805 (1990).

[54] J. I. Cirac, P. Zoller, H. J. Kimble, and H. Mabuchi, *Quantum State Transfer and Entanglement Distribution among Distant Nodes in a Quantum Network*, Phys. Rev. Lett. **78**, 3221 (1997).

[55] F. Reiter and A. S. Sørensen, *Effective Operator Formalism for Open Quantum Systems*, Phys. Rev. A **85**, 032111 (2012).

[56] R. Oulton, B. D. Jones, S. Lam, A. R. A. Chalcraft, D. Szymanski, D. O'Brien, T. F. Krauss, D. Sanvitto, A. M. Fox, D. M. Whittaker, M. Hopkinson, and M. S. Skolnick, *Polarized Quantum Dot Emission from Photonic Crystal Nanocavities Studied under Moderesonant Enhanced Excitation*, Opt. Express **15**, 17221 (2007).

[57] D.-S. Song, Y.-J. Lee, H.-W. Choi, and Y.-H. Lee, *Polarization-Controlled, Single-Transverse-Mode, Photonic-Crystal, Vertical-Cavity, Surface-Emitting Lasers*, Appl. Phys. Lett. **82**, 3182 (2003).

[58] T.-W. Lu, P.-T. Lin, and P.-T. Lee, *Photonic Crystal Horizontally Slotted Nanobeam Cavity for Silicon-Based Nanolasers*, Opt. Lett. **37**, 569 (2012).

[59] Y. Gong and J. Vučković, *Photonic Crystal Cavities in Silicon Dioxide*, Appl. Phys. Lett. **96**, 031107 (2010).

[60] M. W. McCutcheon, P. B. Deotare, Y. Zhang, and M. Lončar, *High-Q Transverse-Electric/Transverse-Magnetic Photonic Crystal Nanobeam Cavities*, Appl. Phys. Lett. **98**, 111117 (2011).

[61] T. P. Mayer Alegre, R. Perahia, and O. Painter, *Optomechanical Zipper Cavity Lasers: Theoretical Analysis of Tuning Range and Stability*, Opt. Express **18**, 7872 (2010).